Available online at www.sciencedirect.com
SCIENCE DIRECT®
International Journal of Mass Spectrometry 228 (2003) 999–1016
International Journal of Mass Spectrometry
www.elsevier.com/locate/ijms

Zinc binding properties of the amyloid fragment Aβ(1–16) studied by electrospray-ionization mass spectrometry

Séverine Zirah[a], Sylvie Rebuffat[a], Sergey A. Kozin[b], Pascale Debey[b], Françoise Fournier[c], Denis Lesage[c], Jean-Claude Tabet[c,*]

[a] *CNRS ESA 8041, USM 502, Chimie et Biochimie des Substances Naturelles, Département Régulations, Développement et Diversité Moléculaire, Muséum National d'Histoire Naturelle, Paris, France*
[b] *Muséum National d'Histoire Naturelle, EA 2703, INRA 806, Paris, France*
[c] *Laboratoire de Chimie Structurale Organique et Biologique, boite 45, Université Paris VI, CNRS UMR 7613, Bâtiment 74, 7ème étage, porte 721, 4, place Jussieu, 75252 Paris Cedex 05, France*

Received 30 December 2002; accepted 25 April 2003

Abstract

A major hallmark of Alzheimer's disease (AD) is the strong accumulation in brain of senile plaques, mainly composed of the amyloid-β peptide (Aβ). Recent studies have suggested that the zinc cation would be a possible key mediating factor for the formation of amyloid extracellular deposits, by binding to Aβ and triggering the involved aggregation process. From a previous circular dichroism (CD) study, we have proposed the N-terminal 1–16 region of Aβ(1–16), as the minimal fragment able to specifically bind zinc. Here we investigate the Zn^{2+} binding properties of Aβ(1–16) by electrospray-ionization mass spectrometry (ESI-MS). The stoichiometry of Aβ(1–16)/Zn^{2+} association and the relative affinity of different cations towards Aβ(1–16) are investigated by analyzing the mass spectra of Aβ(1–16) in the presence of different cations, introduced alone or in competition. Zn^{2+} binding sites are determined from collision-induced dissociation (CID) experiments conducted on the Aβ(1–16) cationized species. From these data, Aβ(1–16) is shown to form a 1:1 complex with Zn^{2+} and to bind up to three cations upon increasing the Zn^{2+} concentration. Under CID, zinc binding induces specific cleavages after the three histidines of the Aβ(1–16) sequence (H^6, H^{13} and H^{14}), showing their simultaneous implication in the Zn^{2+} coordination sphere. The binding of Aβ(1–16) to several Zn^{2+} cations appears less specific, but still implicates the three histidines, each of them behaving thus as an autonomous binding site. A model is proposed to explain both the specific and the aspecific interactions of Zn^{2+} with Aβ(1–16) that is confirmed here to behave as the minimal zinc-binding region of Aβ.

Keywords: Alzheimer's disease; Amyloid peptide; Zinc binding; Electrospray-ionization mass spectrometry

1. Introduction

Amyloid neurotoxic deposition is one of the main cerebral damages associated with Alzheimer's disease (AD). The amyloid peptide Aβ(1–42), which is the major component of these deposits, results from a double proteolytic cleavage of the amyloid precursor

Abbreviations: AD, Alzheimer's disease; APP, amyloid precursor protein; Aβ(1–42), amyloid peptide; Aβ(1–16), N-terminal 1–16 region of Aβ(1–42); CD, circular dichroism

* Corresponding author. Tel.: +33-144-27-31-12; fax: +33-144-27-38-43.
E-mail address: tabet@ccr.jussieu.fr (J.-C. Tabet).

1387-3806/$ – see front matter © 2003 Elsevier Science B.V. All rights reserved.
doi:10.1016/S1387-3806(03)00221-5

protein (APP), a transmembrane glycoprotein widely expressed in a variety of cell types including neurons [1,2]. The above-mentioned enzymatic cleavage is carried out by two proteases, the β- and γ-secretases. Another proteolytic processing pathway that involves both α- and γ-secretases precludes the formation of amyloid peptides, since the α-secretase cleavage takes place between residues 16 and 17 of Aβ, leading to the formation of the non-amyloidogenic Aβ(17–42) [3,4]. Therefore, the amino acid sequence located between the α- and β-secretase cleavage sites appears as required for the amyloid peptide fibrillogenesis.

In the brain, the soluble form of Aβ(1–42) predominantly exists in α-helical and/or unordered conformations, while a β-sheet structure has been characterized within amyloid deposits [5]. Therefore, the Aβ(1–42) transconformation towards β-sheet is supposed to initiate the aggregation step leading to fibrillization. The binding of Aβ(1–42) to metallic ions, and particularly to Zn^{2+}, has been proposed to play a critical role in its aggregation capability [6–8]. This critical role has recently been confirmed by the ability of metal chelatants to decrease amyloid plaques and to inhibit amyloid accumulation in AD transgenic mice [9,10]. Furthermore, many studies reveal an abnormal zinc level in amyloid senile plaques [11,12]. Interestingly, contrary to amyloid deposits that display histochemically detectable zinc ions, preamyloid deposits, which are defined as Aβ non-fibrillar diffuse plaques mainly composed of Aβ(17–42) [13], do not present this histochemical reactivity [14]. This observation suggests that the 1–16 N-terminal region is required for zinc binding that would trigger the amyloidogenic properties. Furthermore, the histidine residues His^6, His^{13} and His^{14}, which all belong to the 1–16 region, have been assumed to be involved in the zinc complexation [15–17].

Unfortunately, biophysical studies carried out on Aβ(1–42) and its fragments, in the absence or in the presence of Zn^{2+} ions, have been often confronted to time and/or Zn^{2+}-induced aggregation in aqueous solution. However, we have recently shown by CD that a synthetic peptide having the amino acid sequence included between the α- and β-secretase cleavage sites, Aβ(1–16), (CH_3CO-DAEFR^{5}HDSGY^{10}EVHHQ^{15}K-NH_2; MW = 1996 Da) formed a soluble and stable complex with Zn^{2+} ions, leading to a conformational change of the peptide [18]. Those findings suggested the Aβ(1–16) region as the minimal autonomous zinc binding domain of Aβ. Delineation of the molecular mechanisms involved in zinc-binding to Aβ(1–16) can thus be considered a key for understanding the resulting fibrillogenesis processes involved in the pathogenicity.

Over the past 10 years, electrospray-ionization mass spectrometry (ESI-MS) has been a growing-up method to study non-covalent interactions [19–23]. Indeed, the gentleness of the desolvation process of ionized aggregates enables to maintain intact weakly bound systems, and many applications suggest that such survivor complexes in the gas phase may nearly reflect, under particular conditions, the interactions as they occur in solution. In the case of amyloid peptides, ESI-MS was used to evidence that Aβ(1–40) selectively interacts with β-cyclodextrin [24] and with melatonin [25], a hormone recently found to inhibit the formation of β-sheets and amyloid fibrils. Recently, Aβ(1–16) with the substitution Glu^{11}Gln was investigated in the presence of Cu^{2+} by metal-catalyzed oxidation conjugated with ESI-MS, allowing to assign the copper binding sites [26]. Binding properties of proteins and peptides with metal ions, and particularly alkali [27,28], alkaline earth [29–31], as well as transition metals [32–51], have been extensively investigated by ESI-MS. These different studies have allowed to determine the stoichiometry of such complexes, and sometimes to characterize a binding-induced conformational change by scrutinizing either the charge state variation of the complexes [29,37] or the H/D exchange extent [30]. Furthermore, the localization of the binding sites could sometimes be achieved either by limited proteolysis in conjunction with ESI-MS monitoring [49] or by analyzing the fragmentation patterns of the complexes under collision-induced dissociation (CID) conditions [31,33,35,36,41,45,50,51].

In the present study, the binding properties of Aβ(1–16) to various metal ions, and particularly to Zn^{2+}, were investigated by ESI-MS, with the aim to

evidence a selective association of Aβ(1–16) to Zn^{2+}. ESI-MS experiments were carried out on Aβ(1–16) in the absence of cations and in the presence of Zn^{2+} and other transition metal ions such as Ni^{2+}, Co^{2+} and Mn^{2+}. The stoichiometry of the metallic peptide complexes and the binding-induced variations of the charge state carried by the Aβ(1–16) species were investigated. Competition experiments between Zn^{2+} and the other selected divalent cations were undertaken in order to assess the relative affinity of the different cations for Aβ(1–16) and the specificity of the Aβ(1–16)/Zn^{2+} interactions. Alternatively, CID experiments were performed on the protonated peptide and on the cationized species, including the adducts with Na^+ and K^+. Comparison between the fragmentation patterns of the peptide, either protonated or in binary complexes with the different cations was used to get complementary information on the location of the metallic ion binding sites within the peptide sequence.

2. Experimental

2.1. Sample preparation

Synthetic peptides (purity > 95%), either acetylated at the N-terminus and amidated at the C-terminus (Aβ(1–16): CH_3CO-DAEFR^{5}HDSGY^{10}EVHHQ^{15}K-NH_2; MW = 1996 Da), or unprotected (Aβ(1–16)^{unp}; MW = 1955 Da), were purchased from Eurogentec (Seraing, Belgium). Samples for ESI-MS were prepared as 10 pmol/μL peptide either in MeOH/H_2O 0:100 to 97:3, or H_2O/i-PrOH 10:90, or 2–10 mM NH_4CH_3COO buffer/MeOH 95:5 at different pH values in the 3–8 range. In experiments performed in the presence of $ZnCl_2$, $NiCl_2$, $MnCl_2$ and $CoCl_2$, the metal to peptide ratios varied from 0:1 to 50:1. In Co^{2+}/Zn^{2+} competition experiments, $CoCl_2$ and $ZnCl_2$ were added to 10 pmol/μL Aβ(1–16) in MeOH/H_2O 97:3 with peptide/Co^{2+}/Zn^{2+} concentration ratios of 1:5:x (x = 0–0.5–1–2–3–4–5). In Ni^{2+}/Zn^{2+} competition experiments, $NiCl_2$ and $ZnCl_2$ were added to 10 pmol/μL Aβ(1–16) in MeOH 100% with peptide/Ni^{2+}/Zn^{2+} ratio of 1:5:5.

2.2. Mass spectrometry

ESI-MS was performed on an Esquire 3000 ion trap mass spectrometer (Bruker Daltonics, Bremen, Germany) fitted with an electrospray source. A syringe pump was used to infuse the solution to the atmospheric pressure ionization source with a gas-tight syringe at a flow rate of 120 μL/h. Positive ion m/z ratio measurements were performed in the 200–2100 Th range, with a 13 and a 1.650 Th/s scan speed for classical experiments and for experiments with enhanced resolution (5000 for 1000 Th), respectively. ESI mass spectra were typically recorded with a 4 kV capillary voltage, a 3.5 kV end plate, and ionization/desolvation conditions were optimized to allow conservation of the produced protonated or cationized complexes over the solvent desolvation at skimmer. CID experiments (MS^2 and MS^3) were performed from selected ion submitted to resonant excitation amplitude from 0.5 to 1.5 V_{P-P}. The selection width was typically 6.0 Th, except for the Zn^{2+}–Co^{2+}-dicationized species for which the precursor ion was selected with a 1 Th width in order to avoid contribution of the Zn^{2+}-dicationized ions in the CID spectra. The reported m/z values for the different ions correspond to the measured m/z ratios. They can be related to either the monoisotopic peak for lower molecular mass ions or to the average m/z ratios for larger molecular mass ions, because of the limited resolution used under our experimental conditions.

3. Results

The cation binding properties of Aβ(1–16) were studied with an electrospray source coupled to an ion trap analysis system that enabled ion structure investigation by multi-stage CID spectra analysis, i.e., MS^n. In order to obtain a good ionization efficiency, MeOH/H_2O 97:3 was chosen as solvent for most experiments, once ensuring that the CID spectra were similar when using different solvent conditions (either MeOH/H_2O 97:3, MeOH/H_2O 50:50 + 0.1% HCOOH or 2 mM ammonium acetate buffer/MeOH 95:5 at different pH values in the 3–6 range). The

common fragmentation pattern observed independently of the solvent used indicated that the initial internal energy was not significantly modified according to the various solvents.

3.1. Desorption and dissociation processes of the multiply-protonated and alkali-cationized Aβ(1–16) and Aβ(1–16)^{unp} species

In the absence of metallic cations, positive ion ESI-MS spectra of Aβ(1–16) (Fig. 1a) and Aβ(1–16)^{unp} in MeOH/H_2O 97:3 to 50:50 displayed multiply-protonated MH_n^{n+} molecules carrying out a maximum charge state of 4+ and 5+, respectively. Under "harder" desolvation conditions (higher skimmer voltage), the ion charge state decreased and more or less extended consecutive ion dissociations appeared, as expected [52,53].

3.1.1. Main dissociation pathways of the Aβ(1–16) multiply-protonated MH_n^{n+} species

CID experiments were performed in the ion trap cell by resonant excitation of the multiply-protonated Aβ(1–16) species carrying various charge states (Fig. 1b–c). The nomenclature introduced by Roepstorff and Folman [54], and further modified by Biemann [55], was adopted here to describe the fragment ions. For internal fragment ions, the general presentation form is $(b_r y_s)_{(r+s-t)}$, where r, s and t indicate the bond cleaved counting from the N-terminus, the bond cleaved from the C-terminus and the total number of amino acid residues in the peptide, respectively. The subscript $(r+s-t)$ thus accounts for the number of residues in the internal fragment. As an example, the internal fragment AEFRHD of Aβ(1–16) has $r = 7$, $s = 15$ and $t = 16$ and is described as $(b_7y_{15})_6$.

Although the complete Aβ(1–16) sequence was not obtained from the product ions, a large distribution of fragment ions was obtained and the presence of diagnostic ions especially allowed to locate the acidic residues. As an example, the CID spectrum of the Aβ(1–16) MH_4^{4+} species displayed mainly the y_{15}^{4+} as base peak, together with the complementary y_9^{2+}/b_7^{2+}, y_5^{2+}/b_{11}^{2+} and $y_3^{+}/(b_{13}^{2+}$ and $b_{13}^{3+})$ and the y_{13}^{3+} multiply-charged ions (Fig. 1b). The selected MH_3^{3+}, MH_2^{2+} (Fig. 1c) and MH^+ parent ions presented a fragmentation pattern similar to that of MH_4^{4+}, with y_{15}^{n+} as base peak for all MH_n^{n+} CID spectra. Additionally, a series of b_i ions, which corresponded to cleavages occurring after the residues V^{12}, H^{13}, H^{14} and Q^{15} was observed, especially in the case of MH_3^{3+} and MH_2^{2+}.

For Aβ(1–16)^{unp}, the proton dispersion appeared reinforced and the corresponding CID spectra of MH_n^{n+} species displayed significant differences in the product ion abundances (data not shown). Furthermore, the favored product ions differed in the CID spectra of Aβ(1–16)^{unp} according to the charge state of the MH_n^{n+} precursor ion (i.e., y_{14}^{4+}, y_5^{2+}, y_9^{2+} and b_7^{+} for MH_5^{5+}, MH_4^{4+}, MH_3^{3+} and MH_2^{2+}, respectively). Such an ion abundance variation upon changing the acetylated N-terminus to the unprotected one has been already observed for several peptides [56] and suggests that the N-terminal group influences peptide bond cleavages, even at long distance [57]. This reflects: (i) a folded conformation of Aβ(1–16) rather than an opened structure, and (ii) long distance proton transfers induced by collisional activation.

Finally, independently of the charge state of the selected multiply-protonated peptide, cleavages at the peptide bonds following the acidic residues (D^1, D^7, E^3 and E^{11}) were significantly enhanced, as previously described for other protonated peptides containing both acidic residues and arginine [58,59]. According to the model proposed by Tsaprailis et al. [59], intramolecular interactions between arginine and acidic residue side chains should favor such specific cleavages. Note that this trend has not been observed previously in the CID spectra of Aβ(1–39) and Aβ(6–39) recorded on a triple quadrupole instrument [60], which displayed abundant b-type ions rather than the diagnostic fragment y_i ions observed here. This trend can be explained by the kinetic shift due to the larger residence time in the ion trap, as compared to that in the triple quadrupole analyzer.

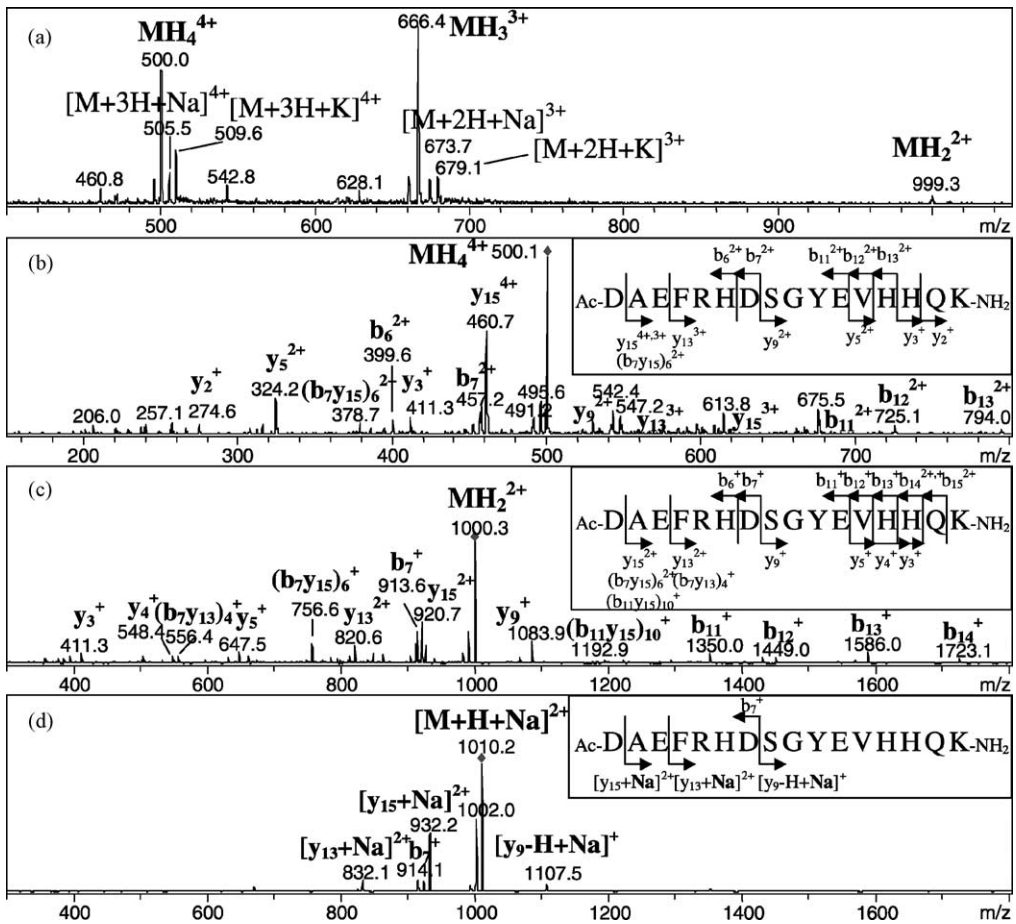

Fig. 1. (a) Positive ion ESI mass spectra of Aβ(1–16), from 10 pmol/μL solution in MeOH/H_2O 97:3. (b)–(d) CID spectra of multiply-protonated and monocationized $[M + H + Na]^{2+}$ Aβ(1–16) species obtained from 10 pmol/μL peptide solution in MeOH/H_2O 97:3. The selected ions are indicated by (♦): (b) MH_4^{4+} (selection of *m/z* 500.0; width 6.0 Th; V_{P-P} 0.65 V); (c) MH_2^{2+} (selection of *m/z* 999.3; width 6.0 Th; V_{P-P} 0.95 V); (d) $[M + H + Na]^{2+}$ (selection of *m/z* 1010.6; width 4.0 Th; V_{P-P} 1.20 V). The main fragmentations displayed on the CID spectra are reported in the insets on the Aβ(1–16) sequence.

MS^3 experiments were performed on fragment ions of MH_n^{n+} (i.e., y_{15} (4+ to 2+) and y_9^{2+}) and the fragmentation patterns were compared to that of the corresponding ions produced directly at the ion source skimmer by "hard" desolvation. The respective CID spectra recorded in the MS^2 mode did not present significant differences relative to the CID mass spectra provided in the MS^3 mode (data not shown). This common behavior towards CID suggested that neither ion structure rearrangement nor charge migration took place over the 10–100 ms duration of the selected ion accumulation into the ion trap cell [61] and thus that a common structure characterized the fragment ions generated from solvated-state ions present in the ion source and from naked ions in the gas phase present in the ion trap.

3.1.2. Main dissociation pathways of the alkali-cationized Aβ(1–16) species

As noted previously, Aβ(1–16) species mono- and dicationized with Na^+ and K^+ were produced by ESI from peptide solution in MeOH/H_2O 97:3. The

presence of these cations was due to alkali traces in solution and/or at the transfer capillary interface. Dissociations of alkali-cationized Aβ(1–16) species, such as $[M + H + Na]^{2+}$ (Fig. 1d), exhibited an improved specificity, as only cleavages at the peptide bonds adjacent to acidic residues occurred, contrasting thus with the CID of the MH_n^{n+} ions that showed a larger product ion distribution. Furthermore, the cationized y_i-type ion series (particularly y_9 and y_{15}) was only obtained, with various charge states. Since the fragmentation experiments were performed at low excitation energy, these specific fragmentations should be induced by the protons rather than by the Na^+ cations. Thus, the alkali-cationized species should be under zwitterionic forms, Na^+ being preferentially located at the deprotonated acidic residues, and protons on the basic sites, such as R^5 and K^{16} side chains in particular. Despite this improved fragmentation specificity, the close fragmentation pattern of the Na^+-cationized Aβ(1–16) species and of the protonated species revealed that binding of the alkali ions did not induce directly specific fragmentations and thus, suggested that these alkali cations played a spectator role.

3.2. Aβ(1–16)/cation complexes

3.2.1. Stoichiometry and charge states of Aβ(1–16)/Zn^{2+} complexes

A previous CD investigation has shown that the Aβ(1–16) peptide undergoes a conformational change in the presence of 2 $ZnCl_2$ equivalents in phosphate buffer, at different pH values in the 6.0–8.0 range, while addition of other cations such as Ca^{2+}, Mg^{2+}, Co^{2+}, Ni^{2+} or Al^{3+} in similar conditions are without effect on the peptide secondary structure [18]. These results suggest that a specific interaction occurs between Aβ(1–16) and Zn^{2+} in solution. The preservation of such a peptide/Zn^{2+} interaction in the gas phase was investigated and evidenced by ESI-MS, with the aim to characterize the binding and in particular to identify the amino acids involved in the coordination. Addition of up to 5 $ZnCl_2$ equivalents to Aβ(1–16) in MeOH/H_2O 97:3 solution yielded ESI mass spectra that displayed intense Aβ(1–16)/Zn^{2+} 1:1 species (Fig. 2a; Table 1), while 1:2 species appeared weak or absent, depending on the source conditions. The presence of bound Zn^{2+} was confirmed by ESI

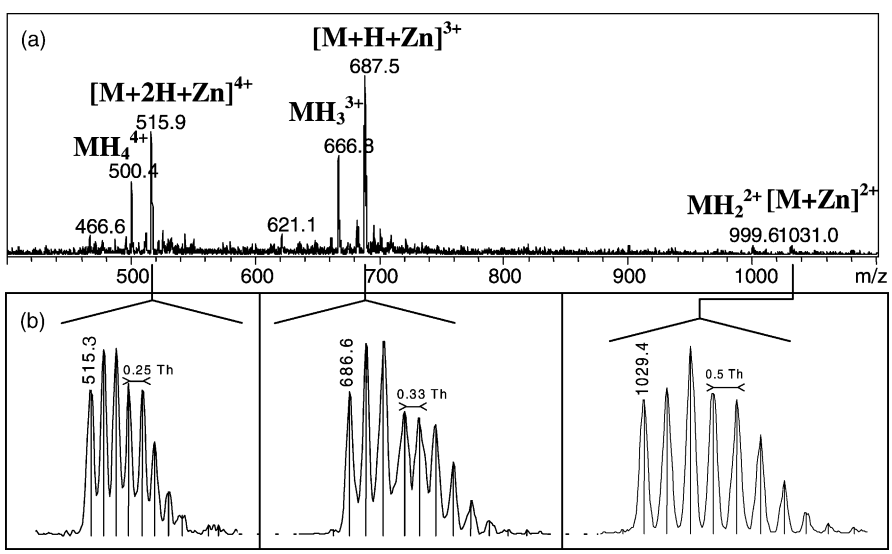

Fig. 2. (a) Positive ion ESI-IT mass spectrum of Aβ(1–16) from 10 pmol/μL peptide solution in MeOH/H_2O 97:3, in the presence of 5 $ZnCl_2$ equivalents. (b) Enlargement of the ESI-IT mass spectra recorded with enhanced resolution from Aβ(1–16)/$ZnCl_2$ 1:5 solution, displaying the isotopic distribution of the Zn^{2+}-cationized species.

Table 1
Relative intensities of the protonated and cationized species displayed on the ESI-IT-MS mass spectra recorded from Aβ(1–16) solutions in the presence of 5 Zn^{2+} or Cat^{2+} equivalents (Cat = Ni, Co or Mn)

Charge state						
Cat^{2+}	4+			3+		
	MH_4^{4+}	$[M + 2H + Cat^{II}]^{4+}$	$[M + 2Cat^{II}]^{4+}$	MH_3^{3+}	$[M + H + Cat^{II}]^{3+}$	$[M - H + 2Cat^{II}]^{3+}$
Zn^{2+}[a]	40.5	69.0	6.1	55.1	100.0	4.5
Ni^{2+}	100.0	91.0	19.9	47.0	92.5	10.4
Co^{2+}	61.1	100.0	46.3	54.4	46.0	19.6
Mn^{2+}	47.3	100.0	28.7	49.6	23.5	8.4

[a] MH_2^{2+} and $[M + Zn^{II}]^{2+}$ are observed on the CID spectrum registered for Aβ(1–16) in the presence of 5 Zn^{2+} equivalents, with a relative intensity of 4.6 and 5.0, respectively.

mass spectra recorded with an enhanced resolution (Fig. 2b), which displayed the natural zinc isotopic distribution contributing to the complexity of the isotopic cluster patterns. Furthermore, the $\Delta m/z$ values between two isotopic peaks confirmed the charge state carried by the different $[M + (n-2)H + Zn^{II}]^{n+}$ species. The charge state was not modified compared to the multi-protonated peptide (i.e., maximum charge state 4+), and the Aβ(1–16)/Zn^{2+} 1:1 complex was the major species for each charge state. Increasing the skimmer voltage led to the formation of either protonated or cationized fragment ions in the ion source, which corresponded to the main fragment ions produced by CID, i.e., y_{15}^{4+} (m/z 460.7) and $[b_{14} - H + Zn^{II}]^{2+}$ (m/z 893.3) (data not shown). At higher Zn^{2+} concentrations, up to 50 equivalents, the production of complexes carrying 1–3 Zn^{2+} ions: $[M + (n-2)H + Zn^{II}]^{n+}$, $[M + (n-4)H + 2Zn^{II}]^{n+}$ and $[M + (n-6)H + 3Zn^{II}]^{n+}$, with n = 2–4 occurred. In addition, the abundance of the multiply-cationized species increased with the charge state.

3.2.2. CID experiments on Aβ(1–16)/Zn^{2+} species

CID spectra of the multiply-charged Aβ(1–16)/Zn^{2+} binary complexes displayed diagnostic ions related to specific cleavages that strongly differed from those observed for the multiply-protonated and the alkali-cationized Aβ(1–16) species (Figs. 3a and 4). Indeed, the Zn^{II}-cationized b_{14} fragment ion emerged from the CID spectra as a base peak, independently of the charge state (n) carried by the selected parent ion ($[b_{14} + Zn^{II}]^{3+}$ for n = 4 and $[b_{14} - H + Zn^{II}]^{2+}$ for n = 2 and 3). It was accompanied by its complementary fragment ion y_2^+ for n = 3 and 4. Except for these common major product ions, the fragmentation pattern was dependent on the parent ion charge state. The CID spectrum of $[M + 2H + Zn^{II}]^{4+}$ (Fig. 3a) displayed four cationized product ions, i.e. $[b_{14} + Zn^{II}]^{3+}$, $[b_{15} + Zn^{II}]^{3+}$, $[b_6 - H + Zn^{II}]^{2+}$ and $[y_{15} + H + Zn^{II}]^{3+}$, the latter being accompanied by its complementary y_{10}^{2+} ion. The CID spectrum of $[M + H + Zn^{II}]^{3+}$ (Fig. 4a) exhibited more various fragmentations: the $[b_{14} - H + Zn^{II}]^{2+}/y_2^+$ and $[b_{13} - H + Zn^{II}]^{2+}/y_3^+$ pairs were observed together with $[b_{15} - H + Zn^{II}]^{2+}$, the $[y_{15} + Zn^{II}]^{3+}$ and $[y_9 - H + Zn^{II}]^{2+}$ y-type cationized fragment ions and the $[(b_{14}y_{15})_{13} - H + Zn^{II}]^{2+}$ cationized internal fragment ion. The CID spectrum of $[M + Zn^{II}]^{2+}$ also displayed more extended fragmentations, with $[b_{14} - H + Zn^{II}]^{2+}$, $[b_{14} - 2H + Zn^{II}]^{+}$, $[b_{13} - 2H + Zn^{II}]^{+}$, $[y_{15} - H + Zn^{II}]^{2+}$ $[(b_{14}y_{15})_{13} - H + Zn^{II}]^{2+}$ and $[(b_{14}y_{13})_{11} - H + Zn^{II}]^{2+}$, together with the $[y_9 - H + Zn^{II}]^{2+}/b_7^+$ pair. The presence of the same diagnostic ions for the different charge states, such as the Zn^{2+}-cationized b_{14}, y_{15} and $(b_{14}y_{15})_{13}$ species, indicated that the Zn^{2+} location did not depend upon the charge state. Note that CID spectra obtained for the unprotected cationized Aβ(1–16)^{unp}/Zn^{2+} were similar to those of the protected Aβ(1–16)/Zn^{2+} complexes (data not shown), which indicated that the N- and C-terminal charges did not influence the specific cleavages observed upon CID on Zn^{2+}-cationized species.

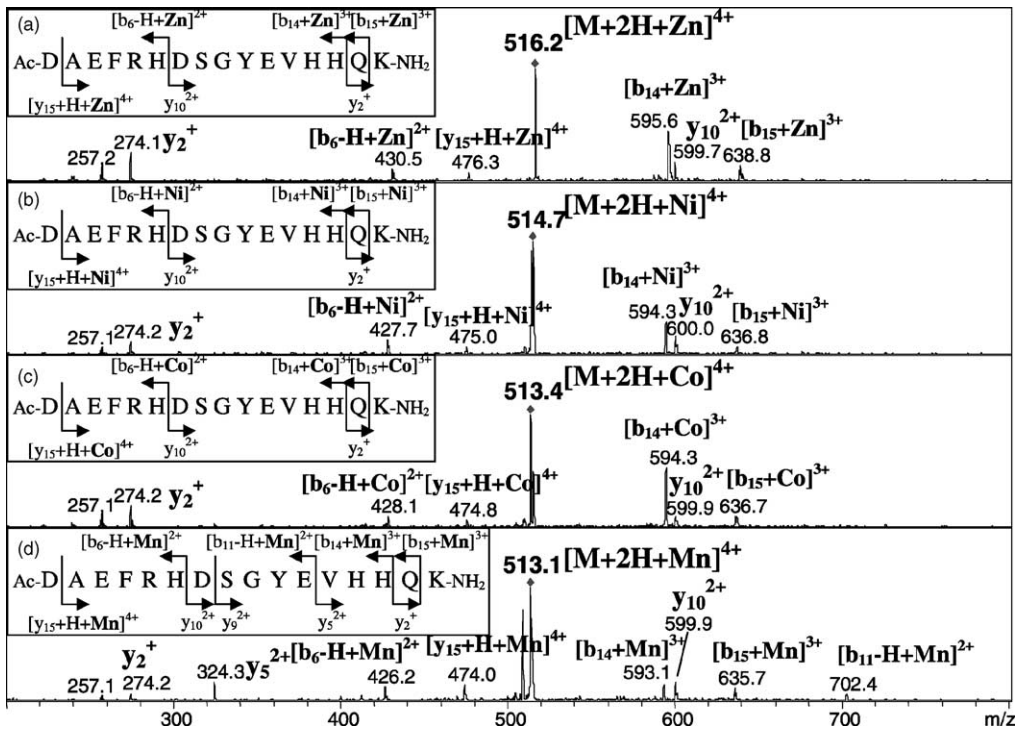

Fig. 3. CID spectra of $[M + 2H + Cat]^{4+}$ cationized Aβ(1–16) species ((a) Cat = Zn, (b) Cat = Ni, (c) Cat = Co, (d) Cat = Mn) obtained from 10 pmol/μL peptide solutions in the presence of 5 Cat^{2+} equivalent in MeOH/H_2O 97:3. The selected ions are indicated by (♦): (a) $[M + 2H + Zn^{II}]^{4+}$ (selection of *m/z* 516.2; width 8.0 Th; V_{P-P} 1.0 V); (b) $[M + 2H + Ni^{II}]^{4+}$ (selection of *m/z* 514.0; width 6.0 Th; V_{P-P} 0.55 V); (c) $[M + 2H + Co^{II}]^{4+}$ (selection of *m/z* 514.0; width 6.0 Th; V_{P-P} 0.55 V); (d) $[M + 2H + Mn^{II}]^{4+}$ (selection of *m/z* 514.0; width 6.0 Th; V_{P-P} 0.55 V).

Additional information could be obtained from sequential multi-stage experiments conducted on the cationized b_{14} fragment ions carried out for different charge states (Table 2). It is worth noting that CID of $[b_{14} - H + Zn^{II}]^{2+}$ and $[b_{14} + Zn^{II}]^{3+}$ fragment ions produced either under "hard" desolvation conditions at the ion source skimmer, or by CID in the ion trap to be selected for sequential MS^3 experiments, resulted in a similar fragmentation pattern. This trend suggested a similar structure of the metallic binary complex in the solvated state and in the gas phase, and the absence of rearrangement of this complex over the period it accumulated in the trap, as shown above for the protonated fragments of Aβ(1–16). The triple-stage MS^3 experiments obtained from the selected $[b_{14} + Zn^{II}]^{3+}$ ion produced by dissociation of $[M + 2H + Zn^{II}]^{4+}$ (Fig. 3a) yielded the cationized $[a_{14} + Zn^{II}]^{3+}$ ion as base peak. The observed loss of CO leading to an a-type ion, indicated that the triply-charged $[b_{14} + Zn^{II}]^{3+}$ fragment ion conserved its linear structure over the process. Furthermore, several species were enhanced, especially the uncationized doubly-charged $b_7{}^{2+}$ ion (47% of the base peak $[a_{14} + Zn^{II}]^{3+}$), accompanied by other uncationized fragment ions, such as $b_8{}^{2+}$, $b_5{}^{+}$ and $(b_7y_{15})_6{}^{2+}$, and by the cationized $[b_6 - H + Zn^{II}]^{2+}$ product ion. These fragment ions relative to N-terminal regions of Aβ(1–16) were observed together with the cationized $[b_{13} - H + Zn^{II}]^{2+}$, $[(b_{14}y_{15})_{13} + Zn^{II}]^{3+}$, $[(b_{14}y_{13})_{11} + Zn^{II}]^{3+}$, $[(b_{14}y_{13})_{11} - H + Zn^{II}]^{2+}$ and $[(b_{14}y_9)_7 - 2H + Zn^{II}]^{+}$ product ions. Triple-stage MS^3 experiments carried out in the same way on $[y_{15} + Zn^{II}]^{3+}$ and $[b_6 - H + Zn^{II}]^{2+}$ also enabled to observe Zn^{2+}-cationized fragment ions, i.e.

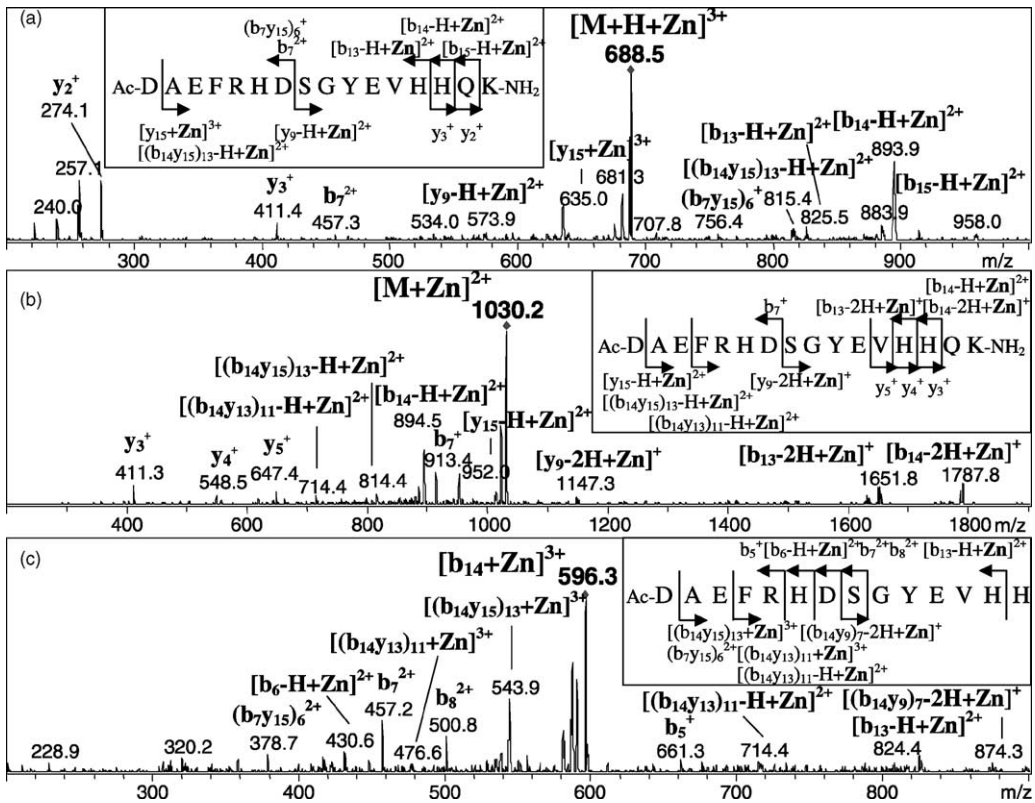

Fig. 4. CID spectra of 1:1 zinc-cationized Aβ(1–16) species obtained from 10 pmol/μL peptide solution in the presence of 5 Zn^{2+} equivalents in MeOH/H_2O 97:3. The selected ions are indicated by (♦): (a) $[M + H + Zn]^{3+}$ (selection of *m/z* 687.1; width 10.0 Th; V_{P-P} 0.75 V); (b) $[M + Zn]^{2+}$ (selection of *m/z* 1031.0; width 6.0 Th; V_{P-P} 1.20 V); (c) MS^3 spectra of $[b_{14} + Zn]^{3+}$ (selection of $[M + 2H + Zn]^{4+}$ *m/z* 515.8; width 10.0 Th; V_{P-P} 0.60 V, followed by that of $[b_{14} + Zn]^{3+}$ *m/z* 596.4; width 10.0 Th; V_{P-P} 0.60 V). For both the sequential MS^2 and MS^3 experiments, the main fragmentations displayed on the CID spectra are reported in the insets on the Aβ(1–16) sequence.

$[(b_{14}y_{15})_{13} - H + Zn^{II}]^{2+}$, $[(b_{14}y_{13})_{11} - H + Zn^{II}]^{2+}$, $[(b_{13}y_{15})_{12} - H + Zn^{II}]^{2+}$, $[y_{13} + Zn^{II}]^{3+}$ and $[y_5 - H + Zn^{II}]^{2+}$ for $[y_{15} + Zn^{II}]^{3+}$ and $[(b_6y_{15})_5 - H + Zn^{II}]^{2+}$, $[(a_6y_{15})_5 - H + Zn^{II}]^{2+}$, $[(a_6y_{14})_4 - H + Zn^{II}]^{2+}$, $[(a_6y_{13})_3 - H + Zn^{II}]^{2+}$ and $[(a_6y_{15})_5 - 2H + Zn^{II}]^{+}$ for $[b_6 - H + Zn^{II}]^{2+}$ (Table 2). The diagnostic Zn^{II}-cationized fragment ions detected under CID conditions enabled to assign two short sequences bound to Zn^{2+}, i.e., $F^4R^5H^6$ and $V^{12}H^{13}H^{14}Q^{15}K^{16}$.

3.2.3. Binding of Aβ(1–16) to other transition metal ions

The specificity of the binding of Aβ(1–16) to Zn^{2+} was investigated by analyzing its binding capability to other transition metal ions, such as Ni^{2+}, Co^{2+} and Mn^{2+}, noted as Cat^{2+}.

Electrospray mass spectra of Aβ(1–16) in the presence of 5 Cat^{2+} equivalents displayed 1:1 and 1:2 Cat^{2+}-cationized Aβ(1–16) species (Table 1). The peptide binding to the metallic cation did not lead to any variation in the charge state, as also noticed for Zn^{2+}. However, unlike the Zn^{2+}-bound species, the Cat^{2+}-cationized Aβ(1–16) species were not the most favored for all the charge states. Indeed, for both Co^{2+} and Mn^{2+}, the 1:1 cationized species was favored for $n = 4$, the multiply-protonated species leading to the major peak for $n = 3$, while in the case of Ni^{2+}, the 1:1 cationized species predominated for

Table 2
Main product ions and relative abundances (related to the base peak of daughter ions) displayed on the MS^3 spectra of zinc-cationized $[b_{14}Zn]^{3+}$, $[y_{15}Zn]^{3+}$ and $[b_6-H+Zn]^{2+}$ fragment ions produced from CID of triply- or quadruply-charged 1:1 Aβ(1–16)/Zn^{2+} complexes, reported on the Aβ(1–16) sequence

Parent ions m/z (V_{P-P})	Neutral loss	Product ions and corresponding monoisotopic m/z (relative intensity)
		Ac - D A E F R H D S G Y E V H H
		$[b_{13}\text{-}H+\mathbf{Zn}]^{2+}$ 824.4 (14.3)
		$[(b_{14}y_{15})_{13}+\mathbf{Zn}]^{3+}$ 543.2 (66.9)
		$[(b_{14}y_{13})_{11}\text{-}H+\mathbf{Zn}]^{2+}$ 714.3 (9.2)
$[M+2H+\mathbf{Zn}]^{4+a}$ 516.1 (0.90)	$[b_{14}+\mathbf{Zn}\text{-}H_2O]^{3+}$ 589.5 (84.5)	$[b_6\text{-}H+\mathbf{Zn}]^{2+}$ 430.6 (17.6) - $[a_6\text{-}H+\mathbf{Zn}]^{2+}$ 416.6 (13.6)
$[b_{14}+\mathbf{Zn}]^{3+b}$ 596.4 (0.70)	$[a_{14}+\mathbf{Zn}]^{3+}$ 586.2 (100.0)	b_8^{2+} 500.7 (32.5)
	$[a_{14}+\mathbf{Zn}\text{-}H_2O]^{3+}$ 580.2 (38.0)	b_7^{2+} 457.2 (47.0) - $[b_7\text{-}H_2O]^{2+}$ 448.2 (10.2)
		$[(b_{14}y_9)_7\text{-}2H+\mathbf{Zn}]^{+}$ 872.3 (7.6)
		b_5^{+} 661.3 (11.5)
		b_3^{+} 358.1 (11.2)
		$(b_7y_{15})_6^{2+}$ 378.7 (16.0)
		$(b_7y_{13})_4^{2+}$ 556.3 (14.8) - $(a_7y_{13})_4^{2+}$ 528.3 (10.6)
		A E F R H D S G Y E V H H Q K - NH_2
		$[(b_{14}y_{15})_{13}\text{-}H+\mathbf{Zn}]^{2+}$ 814.3 (100.0) - $[(b_{14}y_{15})_{13}\text{-}H+\mathbf{Zn}\text{-}H_2O]^{2+}$ 805.3 (37.0)
		y_2^{+} 274.2 (44.7)
		$[(b_{14}y_{13})_{11}\text{-}H+\mathbf{Zn}]^{2+}$ 714.3 (11.5)
		z_2^{+} 257.2 (76.8)
$[M+H+\mathbf{Zn}]^{3+a}$ 687.3 (0.80)		$[z_2\text{-}NH_3]^{+}$ 240.1 (69.3)
		$[z_2\text{-}NH_3\text{-}H_2O]^{+}$ 222.1 (21.5)
$[y_{15}+\mathbf{Zn}]^{3+b}$ 635.7 (0.90)		$[(b_{13}y_{15})_{12}\text{-}H+\mathbf{Zn}]^{2+}$ 878.9 (7.7)
		y_3^{+} 411.2 (12.2)
		$[y_{13}+\mathbf{Zn}]^{3+}$ 567.6 (15.9)
		$(b_7y_{15})_6^{+}$ 756.3 (36.6)
		$[y_5\text{-}H+\mathbf{Zn}]^{2+}$ 355.1 (15.4)
		Ac - D A E F R H
		$[(b_6y_{15})_5\text{-}H+\mathbf{Zn}]^{2+}$ 352.1 (4.5)
		$[(a_6y_{15})_5\text{-}H+\mathbf{Zn}]^{2+}$ 338.1 (35.6)
$[M+2H+\mathbf{Zn}]^{4+a}$ 516.1 (0.95)	$[a_6\text{-}H+\mathbf{Zn}]^{2+}$ 416.6 (100.0)	$[(a_6y_{14})_4\text{-}H+\mathbf{Zn}]^{2+}$ 302.6 (6.9)
$[b_6\text{-}H+\mathbf{Zn}]^{2+b}$ 431.7 (1.00)	$[a_6\text{-}H+\mathbf{Zn}\text{-}H_2O]^{2+}$ 407.6 (25.6)	$[(a_6y_{13})_3\text{-}H+\mathbf{Zn}]^{2+}$ 238.1 (6.8)
		$[(a_6y_{13})_3\text{-}2H+\mathbf{Zn}]^{+}$ 475.2 (11.0)

([a]) Precursor of the selected cationized fragment ion, ([b]) selected cationized fragment ion.

$n = 3$, but not for $n = 4$. This behavior was different from that of 1:1 Zn^{2+}-cationized species, which significantly predominated for each charge state. The strong intensity of $[M + (n - 2)H + Zn^{II}]^{n+}$ species, compared to Aβ(1–16) multiply-protonated species and multiply-cationized species for each charge state $n = 2$–4, indicated that the 1:1 stoichiometry of the Aβ(1–16)/cation complex was favored for Zn^{2+}, while such an 1:1 association appeared less specific for the other cations.

The association of Aβ(1–16) to other cations that was observed in the gas phase did not result in any detectable effect in solution, since the Aβ(1–16) conformational change revealed by CD in the presence of $ZnCl_2$ was not observed any more upon addition of $CoCl_2$ [18]. This illustrates that very slight interactions can be detected by MS and therefore points to the necessity to consider gas-phase results carefully. In our case, competition experiments between the different cations and Zn^{2+} were undertaken to determine the relative affinity of the studied cations for Aβ(1–16) (see subsection 3.2.6.).

3.2.4. Main dissociation pathways of the cationized $[M + (n - 2)H + Cat^{II}]^{n+}$ ions of Aβ(1–16)

CID experiments conducted on the $[M+(n-2)H+Co^{II}]^{n+}$ ($n = 2$–4) species exhibited a fragmentation pattern similar to that of the Aβ(1–16)/Zn^{2+} complexes. This was especially noticeable for the CID spectrum of the quadruply-charged ions, which displayed the same diagnostic ions, i.e., the cationized b_{14} and b_6 fragment ions, although Co^{2+}-cationized species dissociated with a lower resonance excitation energy (Fig. 3c). This result suggested a similar

reactivity of the two cations towards Aβ(1–16), that would thus occupy the same binding sites. CID experiment conducted on $[M + 2H + Ni^{II}]^{4+}$ (Fig. 3b) revealed the same diagnostic ions, but the relative abundances of the cationized $[b_{14} + Ni^{II}]^{3+}$ and $[b_6 - H + Ni^{II}]^{2+}$ ions, together with their y_2^+ and y_{10}^{2+} complementary fragment ions were different, the $[b_6 - H + Ni^{II}]^{2+}/y_{10}^{2+}$ pair being more favored than the corresponding ion pairs for Zn^{2+} and Co^{2+}. The CID spectra of Mn^{2+}-cationized Aβ(1–16) species revealed a more heterogeneous fragmentation pattern, associating metal-induced fragmentations after histidine residues and proton-induced fragmentations after acidic residues (Fig. 3d). From these results, the Aβ(1–16) cation binding sites appeared similar for Zn^{2+}, Co^{2+} and Ni^{2+}, while the Mn^{2+} binding sites showed much lower specificity.

3.2.5. Main dissociation pathways of multiply-cationized $[M + (n - 2m)H + mZn^{II}]^{n+}$ ($m = 2, 3$) and $[M + (n - 4)H + Zn^{II} + Co^{II}]^{n+}$ ions of Aβ(1–16)

CID experiments were performed on Aβ(1–16) multiply-cationized with Zn^{2+}, $[M + (n - 4)H + 2Zn^{II}]^{n+}$ ($n = 3, 4$) and $[M - 2H + 3Zn^{II}]^{4+}$, observed upon increasing the Zn^{2+} concentration up to 50 peptide equivalents. The CID spectrum of $[M+2Zn^{II}]^{4+}$ (Fig. 5a) displayed $[b_{14}-2H+2Zn^{II}]^{3+}$ and its complementary fragment ion y_2^+ as base peaks. The triply-charged b_{14} fragment ion cationized with a single Zn^{2+} ion was also observed, suggesting a more fragile binding of the second Zn^{2+} cation. The spectrum also displayed the $[b_6 - H + Zn^{II}]^{2+}/[y_{10} - H + Zn^{II}]^{2+}$ pair, and the $[y_{15} - H + 2Zn^{II}]^{4+}$ and $[b_{14} - 2H + 2Zn^{II}]^{3+}$ cationized fragment ions, together with the minor fragment ion at *m/z* 987.3. This last ion corresponded either to $[(b_{13}y_{11})_8 - 2H + Zn^{II}]^+$ or to $[(b_{14}y_{10})_8 - 2H + Zn^{II}]^+$, the latter appearing more probable, taking into account the other fragmentations displayed. Note that the $[b_6 - H + Zn^{II}]^{2+}/[y_{10} - H + Zn^{II}]^{2+}$ pair was strongly enhanced compared to the $[b_6 - H + Zn^{II}]^{2+}/y_{10}^{2+}$ pair displayed on the $[M + 2H + Zn^{II}]^{4+}$ CID spectrum (Fig. 3a). CID performed on $[M - H + 2Zn^{II}]^{3+}$ led to highly reduced dissociation efficiency (data not shown). However, minor cationized-fragment ions could be detected, such as $[y_{15} - 2H + 2Zn^{II}]^{3+}$ (*m/z* 655.3), $[b_6 - H + Zn^{II}]^{2+}$ (*m/z* 430.6), $[b_{13} - 3H + 2Zn^{II}]^{2+}$ (*m/z* 855.7), $[b_{14} - 3H + 2Zn^{II}]^{2+}$ (*m/z* 924.3) and $[b_{15} - 3H + 2Zn^{II}]^{2+}$ (*m/z* 988.4). The CID of the triply-cationized $[M - 2H + 3Zn^{II}]^{4+}$ (Fig. 5b) led to the $[b_{14} - 4H + 3Zn^{II}]^{3+}/y_2^+$ and $[b_6 - H + Zn^{II}]^{2+}/[y_{10} - 3H + 2Zn^{II}]^{2+}$ complementary fragment ions.

Considering the CID patterns of the cationized species, the Aβ(1–16) binding properties to Co^{2+} appeared much closer to those observed for Zn^{2+}, compared to Ni^{2+} and Mn^{2+}. Thus, the Co^{2+} cation was selected to further investigate the hetero-dicationized complexes and CID experiments were carried out for the different charge states of the mixed $[M + (n - 4)H + Zn^{II} + Co^{II}]^{n+}$ complexes ($n = 2$–4). The CID spectrum of $[M + Zn^{II} + Co^{II}]^{4+}$ displayed two important features: (i) an identical behavior of Zn^{2+} and Co^{2+} cations, leading to a symmetrical cleavage and (ii) the presence of complementary pairs of product ions, singly-cationized with either Zn^{2+} or Co^{2+} (Fig. 5c). Indeed, $[b_6 - H + Co^{II}]^{2+}$ (*m/z* 428.1) and $[b_6 - H + Zn^{II}]^{2+}$ (*m/z* 430.6) on the one hand, and $[y_{10} - H + Co^{II}]^{2+}$ (*m/z* 628.2) and $[y_{10} - H + Zn^{II}]^{2+}$ (*m/z* 630.7) on the other hand exhibited similar abundances. The two complementary ion pairs, $[b_6 - H + Zn^{II}]^{2+}/[y_{10} - H + Co^{II}]^{2+}$ and $[b_6 - H + Co^{II}]^{2+}/[y_{10} - H + Zn^{II}]^{2+}$ also evidenced the common behavior and reactivity of the Zn^{2+} and Co^{2+} cations. In addition, $[b_{14} - 2H + Zn^{II} + Co^{II}]^{3+}$ was here observed as base peak, similarly to $[b_{14} + Zn^{II}]^{3+}$ and $[b_{14} + Co^{II}]^{3+}$ that were the major ions in the CID spectra of $[M + 2H + Zn^{II}]^{4+}$ and $[M + 2H + Co^{II}]^{4+}$, respectively. Two additional minor ions were observed at *m/z* 982.5 and 987.5. The former could be attributed to a monocharged internal ion, either $(b_{13}y_{11})_8$ or $(b_{14}y_{10})_8$, both being cationized with Co^{2+}, while the latter corresponded to one of these internal fragment ions cationized with Zn^{2+}. From the other fragmentations displayed on the CID spectrum, the $(b_{14}y_{10})_8$ internal ions, i.e. $[(b_{14}y_{10})_8 - 2H + Co^{II}]^+$ and $[(b_{14}y_{10})_8 - 2H + Zn^{II}]^+$, were most probable.

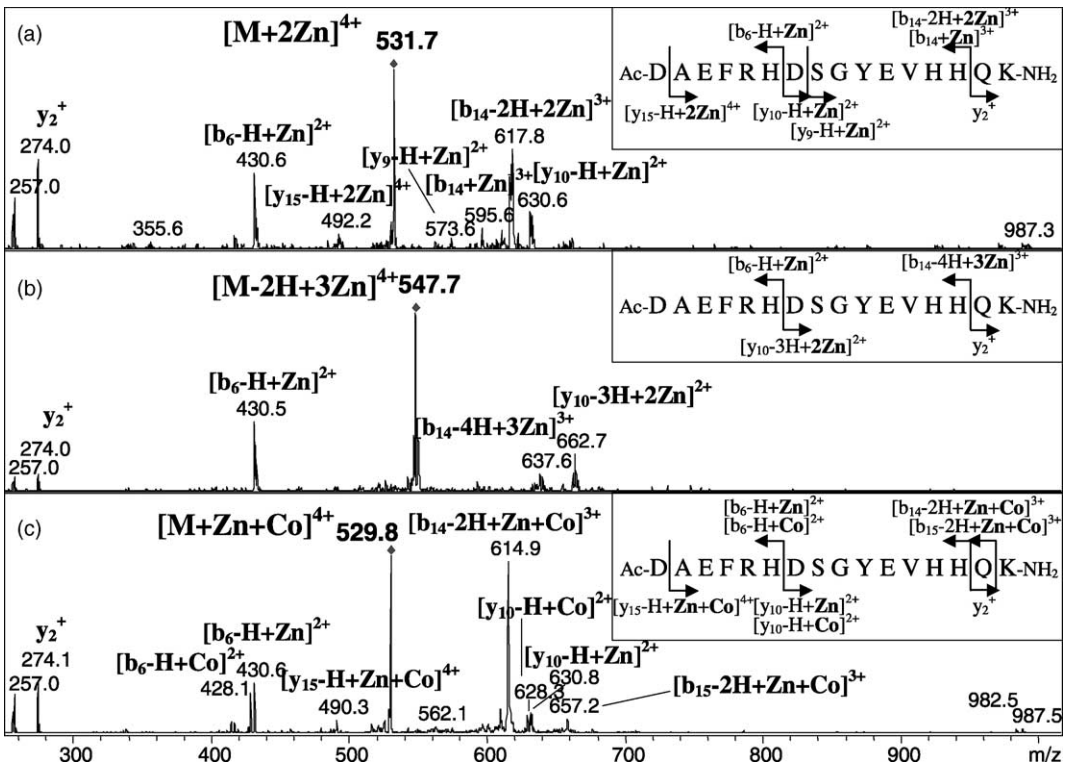

Fig. 5. CID spectra of $[M+(2-m)H+mZn]^{4+}$ multiply-zinc-cationized Aβ(1–16) species obtained from 10 pmol/μL peptide solution in MeOH/H_2O 97:3 in the presence of 10 and 50 Zn^{2+} equivalents for $m=2$ and $m=3$, respectively. (a) $m=2$ (selection of $[M+2Zn]^{4+}$ m/z 531.7; width 6.0 Th; V_{P-P} 1.00 V); (b) $m=3$ (selection of $[M-2H+3Zn]^{4+}$ m/z 547.6; width 10.0 Th; V_{P-P} 0.90 V). (c) CID spectrum of $[M+Zn+Co]^{4+}$ obtained from 10 pmol/μL Aβ(1–16) solution with peptide/Zn^{2+}/Co^{2+} concentration ratio 1:4:5 in MeOH/H_2O 97:3 (selection of $[M+Zn+Co]^{4+}$ m/z 529.7; width 1.0 Th; V_{P-P} 0.60 V). For each CID spectrum, the selected ion is indicated by (♦), and the main fragmentations are reported in the insets on the Aβ(1–16) sequence.

Therefore, CID experiments conducted on the $[M+(n-4)H+Zn^{II}+Co^{II}]^{n+}$ and $[M+(n-4)H+2Zn^{II}]^{n+}$ species provided further evidence of a similar binding of the Co^{2+} and Zn^{2+} cations to Aβ(1–16). To determine the relative affinity of Zn^{2+} and Co^{2+} to Aβ(1–16), competition experiments were finally undertaken.

3.2.6. Relative affinities of Aβ(1–16) for the different cations, from Zn^{2+}/Co^{2+} competition experiments

At first, the relative affinity of Aβ(1–16) for Zn^{2+} and Co^{2+} was examined in the presence of 5 Co^{2+} equivalents and of increasing Zn^{2+} concentrations (0.5–5 equivalents). The intensity of the cationized ions displayed on the mass spectra as regard the Zn^{2+}/peptide ratio (Fig. 6) clearly revealed a stronger affinity of Aβ(1–16) to Zn^{2+}, since the Zn^{2+}-cationized Aβ(1–16) was the major species for 1:5:1 to 1:5:5 Aβ(1–16)/Co^{2+}/Zn^{2+} ratios. Moreover, the intensities of the Zn^{2+}-homodicationized and Zn^{2+}/Co^{2+}-heterodicationized Aβ(1–16) species were similar from a 1:5:3 Aβ(1–16)/Co^{2+}/Zn^{2+} proportion. Therefore, this competition experiment indicated (i) a lower affinity of Aβ(1–16) for Co^{2+} than for Zn^{2+} and (ii) the absence of specificity for the binding of a second Zn^{2+} cation to Aβ(1–16). Mass spectra recorded for Aβ(1–16) in the presence of Zn^{2+} and Ni^{2+} with a 1:5:5 Aβ(1–16)/Ni^{2+}/Zn^{2+} ratio revealed also a stronger affinity for Zn^{2+}, since

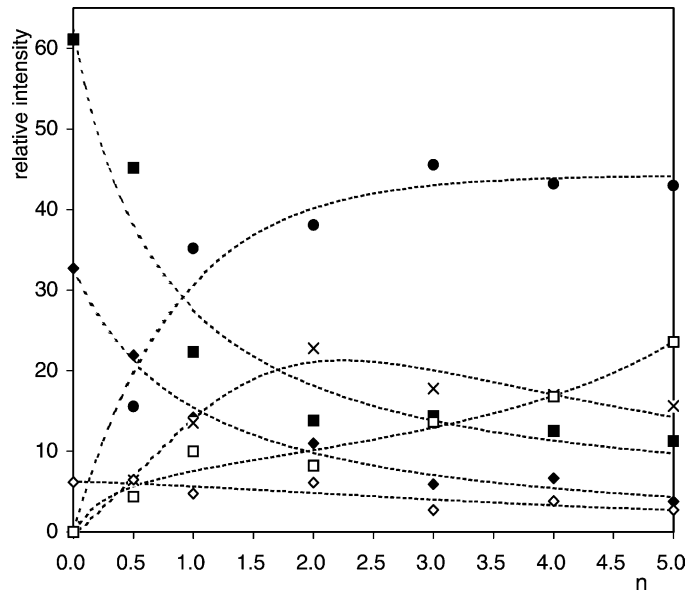

Fig. 6. Variation of the relative intensity of the protonated, singly- and doubly-cationized Aβ(1–16) species as a function of the Zn^{2+}/Aβ(1–16) concentration ratio (Aβ(1–16)/Co^{2+}/Zn^{2+} concentration ratio = 1:5:*n* with *n* = 0–5). The intensity of all the charge states displayed are summed for each considered species. (■): multi-protonated species, (●): Zn^{II}-monocationized species, (◆): Co^{II}-monocationized species, (□): Zn^{II}-dicationized species, (◇): Co^{II}-dicationized species, (×): Zn^{II}–Co^{II}-dicationized species.

Ni^{2+}-cationized species were negligible compared to Zn^{2+}-cationized species (data not shown).

4. Discussion

The present study was undertaken to characterize by ESI-IT-MS the binding properties of Aβ(1–16) to Zn^{2+} that has been pointed previously in solution by CD [18] and to define the location of the interaction sites between the peptide and the Zn^{2+} cation. The particular selectivity of this Zn^{2+} association compared to that with different other transition metal cations was evidenced, and Aβ(1–16)/Zn^{2+} binding sites were investigated through CID experiments by studying the fragmentation patterns of protonated Aβ(1–16), associated (or not) to different cations including Zn^{2+}. The predominant stoichiometry of one Zn^{II} in the metal/Aβ(1–16) complex has been directly shown from ESI mass spectra. The specificity of Zn^{2+} binding has been investigated by analyzing the peptide behavior towards other transition metals, i.e., Ni^{2+}, Co^{2+} and Mn^{2+}, that revealed similar binding properties for Zn^{2+} and Co^{2+}. However, competition experiments revealed a much lower affinity of the Co^{2+} cation for Aβ(1–16), compared to Zn^{2+}.

4.1. Determination of Zn^{II} binding sites from CID experiments

The orientation of the dissociations of zinc-cationized Aβ(1–16) species upon CID strongly differs from that of the corresponding multiply-protonated and alkali-cationized species. As an example, despite the largest charge state carried by the $[M + 2H + Zn^{II}]^{4+}$ selected ion, it shows a particular stability towards collisions and only a few characteristic dissociation patterns emerge from its CID spectrum (Fig. 3a). The observed product ions correspond to specific cleavages at the H^{14}–Q^{15}, H^{6}–D^{7} and Q^{15}–K^{16} peptide bonds, leading to b-type cationized fragment ions. This behavior contrasts with that exhibited by multiply-protonated species and alkali cation multiply-charged complexes. Indeed, the former

species yield a large number of product ions, leading to the incomplete y_i and b_j series, fragmentations at cleavage sites located after the acidic residues being favored, while the latter species exhibit limited fragmentations, dissociations only occurring at peptide bonds that follow the acidic residues. In the case of Zn^{2+}-cationized species, such regiospecific fragmentations only related to the amino acid sequence are replaced by regiospecific fragmentations after the histidine residues that are triggered by cation binding, as already observed for other histidine-containing peptides [33,35]. This change in the fragmentation pattern upon zinc binding suggests that Zn^{II} is linked to the considered histidine, and thus initiates the cleavage of the following bond under CID conditions. Histidine is known as a residue favoring zinc attachment, as illustrated by its implication in numerous zinc binding motifs [62]. In the gas-phase, Zn^{2+} interaction with amino acids is well documented [63–70] and the cationization of histidine has been especially described [63–65,67]. Histidine/Zn^{II} binding is maintained in the gas phase under soft desolvation conditions. Moreover, this interaction is enhanced by the strong acidity of histidine in the gas phase [71]. The unexpected gas-phase acidity of the free histidine is related to a major extent to its carboxylic group, but should also implicate the side-chain imidazole group, which has a strong amphoteric character. This acidic property is illustrated by the observation of neutral [72] and deprotonated imidazole [73] in metal–peptide complexes observed by negative-mode ESI-MS. Therefore, an acidic property of the residue when involved in a peptidic sequence can be assumed, which would favor the formation of zwitterionic systems, thus providing strongly stabilized structures.

Here we have investigated the location of the Zn^{2+} binding sites by analyzing the fragmentation patterns of the peptide–Zn^{2+} species. The similar fragmentation pattern of the Zn^{2+}-cationized b_{14} species, either produced in the source from solvated species or under dissociations in the analyzer from naked cationized species, confirmed the possibility to determine very carefully the zinc binding sites in solution from gas-phase CID experiments, since no rearrangement of the cationized $[M + (n - 2)H + Zn^{II}]^{n+}$ species appeared to occur over the period they accumulated in the trap. Independently of the charge state, CID of the $[M+(n-2)H+Zn^{II}]^{n+}$ cationized species yields the zinc-cationized b_{14} product ion as base peak. This diagnostic peak indicates that the H^{14} residue participates in the binding of Zn^{2+} to Aβ(1–16) that results in Zn^{2+}-induced fragmentations. The presence of its complementary $y_2{}^+$ fragment ion, for $n = 3$ and 4, shows that the C-terminal lysine residue is protonated in the corresponding precursor ions. The presence of the minor $[b_6 - H + Zn^{II}]^{2+}$ fragment ion in the $[M + 2H + Zn^{II}]^{4+}$ CID spectrum (Fig. 3a) must be emphasized, since it suggests the possible contribution of H^6 to the Zn^{II} coordination sphere, in addition to the above-mentioned H^{14}. Nevertheless, the region encompassing D^1 to H^6 does not appear as an autonomous binding site, since the CID spectra of the Aβ(1–16)/Zn^{2+} complexes show that the corresponding fragment ions are either weak or absent, depending on the charge state. Contrasting with this result, the presence of the $[y_9-H+Zn^{II}]^{2+}$ and $[y_9-2H+Zn^{II}]^+$ fragment ions in the CID spectrum of the triply- and doubly-charged complexes, respectively, indicates that the Zn^{2+} cation is located in the region encompassing S^8 to K^{16}. Additional information could be obtained from multi-stage MS^3 experiments on the cationized b_{14} fragment ions. Indeed, the presence of both protonated and cationized N-terminal product ions indicates that consecutively to CID, the Zn^{2+} cation remains attached either on the N-terminal region, implicating the H^6 residue, or on the C-terminal region, implicating the H^{13} and/or H^{14} residues. However, the presence of intense N-terminal uncationized product ions suggests that the Zn^{2+} association with H^6 is weaker than that with H^{13}/H^{14}. Altogether, the fragmentation patterns of $[M+(n-2)H+Zn^{II}]^{n+}$ and of the cationized b_{14} species (Figs. 3a and 4; Table 2) suggest that prior to dissociation, Zn^{II} is located in the proximity of the three histidines H^6, H^{13} and H^{14}. This assumption is confirmed by MS^3 experiments carried out on $[b_6 - H + Zn^{II}]$ and $[y_{15} + Zn^{II}]^{3+}$, which enable to assign the F^4–H^6 and the V^{12}–K^{16} segments as minimal binding regions encompassing

the N- and C-terminal domains, respectively. The presence of the cationized b_{14} fragment ion as major product ion on the CID spectra of Zn^{2+}-cationized Aβ(1–16) species suggests that this last region can be reduced to the minimal V^{12}–H^{14} binding domain.

4.2. Model proposed for the Aβ(1–16)/Zn^{2+} binary complex

Therefore, the specific fragmentations of the peptide/Zn^{2+} species have allowed to propose a model for the Zn^{II} cation binding to Aβ(1–16), involving the three histidine residues of the peptide sequence. We hypothesize the additional contribution of R^5 to the coordination sphere, thus resulting in a tetrahedral coordination site that implicates four residues assembled into two pairs, R^5–H^6 and H^{13}–H^{14} (Scheme 1). Excitation would thus lead to a partial dissociation of the complex, with attachment of Zn^{II} to either the R^5–H^6 pair or the H^{13}–H^{14} pair. In such a model, Zn^{2+} has a higher tendency to bind to the H^{13}–H^{14} pair than to the R^5–H^6 one, due to the strong basicity of R^5 [71] that likely favors proton attachment at its side chain and consequently destabilizes Zn^{2+} binding. The proposed complex would adopt a folded conformation, favored by the Zn^{II} coordination to both the H^{13}–H^{14} pair and the H^6 residue. The proposed model is in agreement with the fragmentation patterns of the multiply-charged doubly-cationized complexes. Positive charges would be located on the C-terminal lysine in the case of cationized species carrying 3 and 4 charge states, as illustrated by the presence of the intense $y_2{}^+$ fragment ion on the corresponding CID spectra. Finally, the results obtained for Aβ(1–16) in the presence of Co^{2+} alone or in competition with Zn^{2+} suggest that the two cations compete for the same binding sites, but that the Co^{2+} ion has a lower affinity for Aβ(1–16) than Zn^{2+}. CID experiments carried out on Ni^{2+}-cationized species, which also display the b_{14} and b_6 cationized product ions, but with an enhanced $[b_6 - 2H + Ni^{II}]^{2+}/y_{10}{}^{2+}$ pair, suggest that Ni^{2+} binds either the D^1–H^6 region or the D^7–H^{14} region. On the contrary, Mn^{2+} binding sites appear more delocalized, as shown by the heterogeneity of the cationized species obtained in the CID experiments.

4.3. Multiple cation binding to Aβ(1–16)

CID spectra of the dicationized Aβ(1–16) species indicate that the binding of a second cation to Aβ(1–16) (either Zn^{2+} or Co^{2+}) results in the presence of two autonomous binding sites, encompassing the A^2–H^6 and the D^7–H^{14} regions, respectively. In the case of Zn^{2+}-dicationized species, this is illustrated by the $[b_6 - H + Zn^{II}]^{2+}$ and $[y_{10} - H + Zn^{II}]^{2+}$ fragment ions, which are strongly enhanced in the case of the CID spectrum of $[M + 2Zn^{II}]^{4+}$ (Fig. 5a), compared to the $[b_6 - H + Zn^{II}]^{2+}/y_{10}{}^{2+}$ pair displayed on the CID spectrum of the singly-cationized $[M + 2H + Zn^{II}]^{4+}$ (Fig. 3a). This behavior can be explained by considering that the R^5–H^6 pair coordinates one Zn^{2+}, while the second Zn^{2+} cation is bound to the H^{13}–H^{14} pair. Such an assumption implies that one (or several) residue(s) are in the zwitterionic form, thus allowing a strong Zn^{2+} binding to the deprotonated histidines. In the case of Co^{2+}/Zn^{2+}-dicationized species, the two binding regions exhibit similar reactivity towards Co^{2+} and Zn^{2+}, as illustrated by the symmetry in the fragmentation pattern (Fig. 5c). This provides further evidence that Zn^{2+} and Co^{2+} share similar binding properties to Aβ(1–16).

Finally, the CID experiments that were acquired in the presence of a Zn^{2+} excess with the Aβ(1–16)/Zn^{2+} complex 1:3 species (Fig. 5b) indicate three autonomous Zn^{2+} binding sites along the Aβ(1–16) sequence. Indeed, the presence of the $[b_6 - H + Zn^{II}]^{2+}$ and $[y_{10} - 3H + 2Zn^{II}]^{2+}$ ions on the CID spectrum of $[M - 2H + 3Zn^{II}]^{4+}$ species shows that one Zn^{2+} cation is located in the A^2–H^6 region, while the two other Zn^{2+} cations are located in the D^7–H^{14} region. These results suggest that each histidine might constitute independently a Zn^{2+} binding site when several Zn^{2+} cations are attached to Aβ(1–16), while the three histidines should participate together in the coordination sphere when a single Zn^{2+} ion binds to Aβ(1–16). The observation of both the N- and

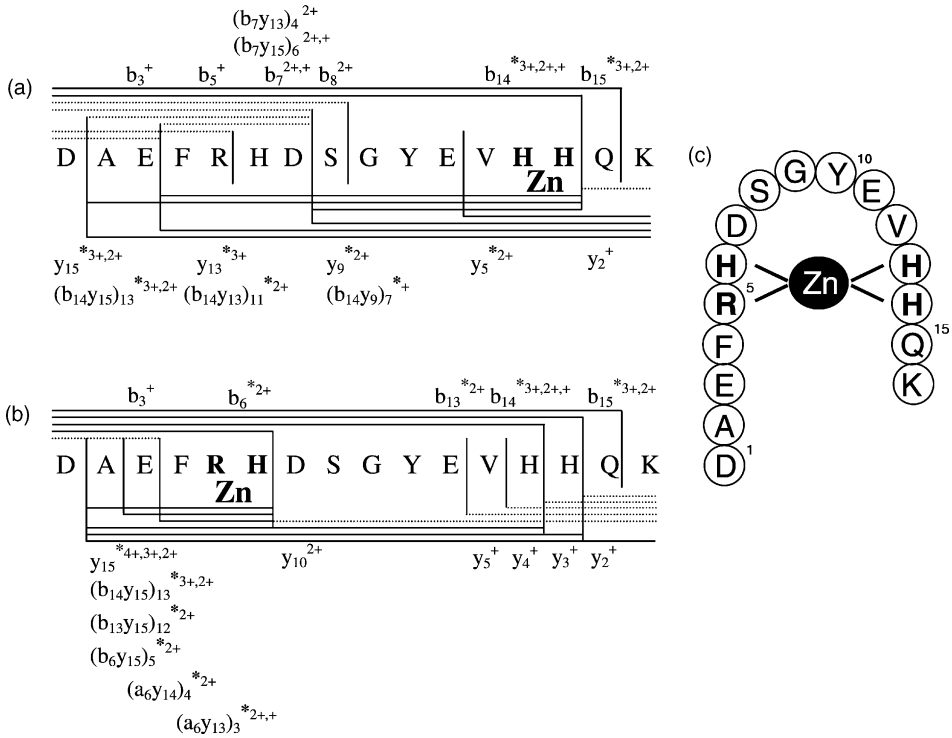

Scheme 1. Hypothesis of Zn^{2+} location for the 1:1 complex after excitation, explaining the different cationized and protonated product ions observed upon CID and MS^3 experiments on cationized fragment ions of the 1:1 Aβ(1–16)/Zn^{2+} complexes. Protonated and cationized fragment ions illustrating (a) the Zn^{2+} location on the S^8–H^{14} C-terminal region and (b) the Zn^{2+} location on the A^2–H^6 N-terminal region. Solid lines refer to zinc-cationized fragment ions and dotted lines refer to uncationized fragment ions. The metal ion is omitted from the label for simplicity, and cationized fragments are designated by a superscript (*). Again for simplicity, the number of donated or accepted protons is not mentioned, but can be easily deduced from the charge state. (c) Model of the cationized Aβ(1–16)/Zn^{2+} binary complex, hypothesized regarding to the fragmentation patterns of the 1:1, 1:2 and 1:3 Aβ(1–16)/Zn^{2+} complexes upon CID.

C-terminal cationized-fragment ions on the CID spectra of the $[M + (n - 2)H + Zn^{II}]^{n+}$ species (Figs. 3a and 4; Scheme 1) illustrates this last point.

Altogether, these results indicate that (i) Aβ(1–16) has a strong affinity for Zn^{2+}, compared to the other considered cations, and (ii) the binding of one Zn^{2+} cation involves the simultaneous implication of the three H^6, H^{13} and H^{14} histidines, thus resulting in a folded structure of the peptide. Such a folded conformation was already pointed in the absence of Zn^{2+}, when analyzing the fragmentation pattern of the unprotected peptide, thus suggesting that Zn^{2+} does not induce this folding, but rather stabilizes it. Note that the same site of interaction was recently described for Cu^{2+} binding to an Aβ(1–16) variant including the mutation $Glu^{11}Gln$, by using metal-catalyzed oxidation combined with ESI-MS [26]. Additional binding that can result from the presence of zinc excess or of other cations, occurs without specificity for Zn^{2+}. This multiple ion binding involves the three histidines again, but this time the A^2–H^6 and D^7–H^{14} regions act as autonomous binding sites, a zwitterionic form that involves deprotonated histidine residues being implied.

5. Conclusions

The Aβ(1–16) peptide, the sequence of which is included between the α- and β-secretase cleavage sites

of APP, is hypothesized to be a key component of the pathogenic transconformation processes involved in Alzheimer's disease. In particular, the binding of Aβ(1–16) to the Zn^{2+} cation could be one of the main events involved in the transconformation that could trigger amyloid deposition. Our previous CD study allowed to propose Aβ(1–16) as the minimal zinc-binding fragment of Aβ [18]. Electrospray ionization was shown here to be very useful by its fast and accurate measurements for direct determination of metallic ion binding to a substrate such as Aβ(1–16). Such complexes were preserved in gas phase after soft desolvation by using adequate solvent conditions.

This MS study of Aβ(1–16) in presence of several cations compared to Zn^{2+} revealed a specific 1:1 association between Aβ(1–16) and Zn^{2+}, which can reflect the intrinsic stoichiometry of the complex in solution. ESI combined with tandem mass spectrometry permitted to evidence and to compare the interactions between Aβ(1–16) and various metallic cations. Indeed, CID experiments of the survivor multiply-charged Aβ(1–16)/Zn^{2+} complexes resulted in strong specific dissociations involving the bonds vicinal to H^{13}–H^{14} and R^5–H^6 that occurred in the case of the complexes carrying 3 or 4 charges. It can thus be proposed that the Aβ(1–16)/Zn^{2+} 1:1 complex adopts a hairpin-like conformation that involves the R^5–H^6 and H^{13}–H^{14} pairs coordinating altogether Zn^{II}, without the contribution of the N- and C-termini.

The mass spectrometry data obtained here on the Aβ(1–16)/Zn^{2+} complex preserved in the gas-phase are in agreement with our previous observations in solution from CD measurements that they substantially complete, thus providing direct evidence of the zinc binding sites. The role of the 1–16 N-terminal part of the amyloid peptide as an autonomous zinc-binding region appears here reinforced. The C-terminal region of the full-length amyloid peptide Aβ(1–42) is highly hydrophobic and presents a potential intrinsic ability to aggregate. Zinc binding to the 1–16 N-terminal region of Aβ(1–42) could be critical in the initiation of the amyloidogenesis by yielding intra- and intermolecular associations that could favor the aggregation step leading to amyloid deposition.

References

[1] D.J. Selkoe, Ann. Rev. Neurosci. 17 (1994) 489.
[2] M.P. Mattson, Physiol. Rev. 77 (1997) 1081.
[3] E. Gowing, A.E. Roher, A.S. Woods, R.J. Cotter, M. Chaney, S.P. Little, M.J. Ball, J. Biol. Chem. 269 (1994) 10987.
[4] M.P. Mattson, Nat. Struct. Biol. 2 (1995) 926.
[5] L.-P.I. Choo, D.L. Wetzel, W.C. Halliday, M. Jackson, S.M. LeVine, H.H. Mantsch, Biophys. J. 71 (1996) 1672.
[6] A.I. Bush, W.H. Pettingell, G. Multhaup, M.D. Paradis, J.P. Vonsattel, J.F. Gusella, K. Beyreuther, C.L. Masters, R.E. Tanzi, Science 265 (1994) 1464.
[7] X. Huang, M.P. Cuajungco, C.S. Atwood, R.D. Moir, R.E. Tanzi, A.I. Bush, J. Nutr. 130 (2000) 1488S.
[8] M.P. Cuajungco, K.Y. Fagét, Brain Res. Rev. 41 (2003) 44.
[9] A.I. Bush, Neurobiol. Aging 23 (2002) 1031.
[10] R.A. Cherny, C.S. Atwood, M.E. Xilinas, D.N. Gray, W.D. Jones, C.A. McLean, K.J. Barnham, I. Volitakis, F.W. Fraser, Y.-S. Kim, X. Huang, L.E. Goldstein, R.D. Moir, J.T. Tim, K. Beyreuther, H. Zheng, R.E. Tanzi, C.L. Masters, A.I. Bush, Neuron 30 (2001) 665.
[11] S.W. Suh, K.B. Jensen, M.S. Jensen, D.S. Silva, P.J. Kesslak, G. Danscher, C.J. Frederickson, Brain Res. 852 (2000) 274.
[12] J.D. Robertson, A.M. Crafford, W.R. Markesbery, M.A. Lovell, Nucl. Instr. Meth. Phys. Res. B 189 (2002) 454.
[13] M. Lalowski, A. Golabek, C.A. Lemere, D.J. Selkoe, H.M. Wisniewski, R.C. Beavis, B. Frangione, T. Wisniewski, J. Biol. Chem. 271 (1996) 33623.
[14] J.-Y. Lee, I. Mook-Jung, J.-Y. Koh, J. Neurosci. 19 (1999) RC10.
[15] S.T. Liu, G. Howlett, C.J. Barrow, Biochemistry 38 (1999) 9373.
[16] T. Miura, K. Suzuki, N. Kohata, H. Takeuchi, Biochemistry 39 (2000) 7024.
[17] D.S. Yang, J. McLaurin, K. Qin, D. Westaway, P.E. Fraser, Eur. J. Biochem. 267 (2000) 6692.
[18] S.A. Kozin, S. Zirah, S. Rebuffat, G. Hui Bon Hoa, P. Debey, Biochem. Biophys. Res. Commun. 285 (2001) 959.
[19] R.D. Smith, K.J. Light-Wahl, Biol. Mass Spectrom. 22 (1993) 493.
[20] M. Przybylski, M.O. Glocker, Angew Chem. Int. Ed. Engl. 35 (1996) 806.
[21] J.A. Loo, Mass Spectrom. Rev. 16 (1997) 1.
[22] B.N. Pramanik, P.L. Bartner, U.A. Mirza, Y.-H. Liu, A.K. Ganguly, J. Mass Spectrom. 33 (1998) 911.
[23] J.A. Loo, Int. J. Mass Spectrom. 200 (2000) 175.
[24] P. Camilleri, N.J. Haskins, D.R. Howlett, FEBS Lett. 341 (1994) 256.
[25] Z. Skribanek, L. Baláspiri, M. Mák, J. Mass Spectrom. 36 (2001) 1226.
[26] J. Lim, R.W. Vachet, Anal. Chem. 75 (2003) 1164.
[27] M. Kanai, A. Iida, Y. Nagaoka, S. Wada, T. Fujita, J. Mass Spectrom. 31 (1996) 177.
[28] L.C.M. Ngoka, M.L. Gross, J. Mass Spectrom. 35 (2000) 265.
[29] T.D. Veenstra, K.L. Johnson, A.J. Tomlinson, R. Kumar, S. Naylor, Rapid Commun. Mass Spectrom. 12 (1998) 613.

[30] F. Halgand, R. Dumas, V. Biou, J.P. Andrieu, K. Thomazeau, J. Gagnon, R. Douce, E. Forest, Biochemistry 38 (1999) 6025.
[31] O.V. Nemirovskiy, M.L. Gross, J. Am. Soc. Mass Spectrom. 9 (1998) 1020.
[32] A. Surovoy, D. Waidelich, G. Jung, FEBS Lett. 311 (1992) 259.
[33] J.A. Loo, P. Hu, R.D. Smith, J. Am. Soc. Mass Spectrom. 5 (1994) 959.
[34] A. Reiter, J. Adams, H. Zhao, J. Am. Chem. Soc. 116 (1994) 7827.
[35] P. Hu, J.A. Loo, J. Am. Chem. Soc. 117 (1995) 11314.
[36] M.C. Sullards, J. Adams, J. Am. Soc. Mass Spectrom. 6 (1995) 608.
[37] H.E. Witkowska, C.H.L. Shackleton, K. Dahlman-Wright, J.Y. Kim, J.-A. Gustafsson, J. Am. Chem. Soc. 117 (1995) 3319.
[38] P.L. Gadhavi, FEBS Lett. 417 (1997) 145.
[39] D. Fabris, Y. Hathout, C. Fenselau, Inorg. Chem. 38 (1999) 1322.
[40] J. Volz, F.U. Bosch, M. Wunderlin, M. Schuhmacher, K. Melchers, K. Bensch, W. Steinhilber, K.P. Schäfer, G. Tóth, B. Penke, M. Przybylski, J. Chromatogr. A 800 (1998) 29.
[41] O.V. Nemirovskiy, M.L. Gross, J. Am. Soc. Mass Spectrom. 9 (1998) 1285.
[42] P.A. Guy, R.J. Anderegg, A. Lim, M.J. Saderholm, Y. Yan, B.W. Erickson, J. Am. Soc. Mass Spectrom. 10 (1999) 969.
[43] D. Brewer, G. Lajoie, Rapid Commun. Mass Spectrom. 14 (2000) 1736.
[44] R.M. Whittal, H.L. Ball, F.E. Cohen, A.L. Burlingame, S.B. Prusiner, M.A. Baldwin, Protein Sci. 9 (2000) 332.
[45] J. Lippincott, T.J. Fattor, D.D. Lemon, I. Apostol, Anal. Biochem. 284 (2000) 247.
[46] L.A. Morris, M. Jaspars, J.J. Kettenes-van den Bosch, K. Versluis, A.J.R. Heck, S.M. Kelly, N.C. Price, Tetrahedron 57 (2001) 3185.
[47] A.H. Payne, G.L. Glish, Int. J. Mass Spectrom. 204 (2001) 47.
[48] T.A. Craig, L.M. Benson, S. Naylor, R. Kumar, Rapid Commun. Mass Spectrom. 15 (2001) 1011.
[49] J.A. Loo, Int. J. Mass Spectrom. 204 (2001) 113.
[50] R.W. Vachet, J.R. Hartman, J.W. Gertner, J.H. Callahan, Int. J. Mass Spectrom. 204 (2001) 101.
[51] C. Afonso, Y. Hathout, C. Fenselau, J. Mass Spectrom. 37 (2002) 755.
[52] L. Drahos, R.A.A. Heeren, C. Collette, E. De Pauw, K. Vékey, J. Mass Spectrom. 34 (1999) 1373.
[53] A.G. Harrison, Rapid Commun. Mass Spectrom. 13 (1999) 1663.
[54] P. Roepstorff, J. Fohlman, Biomed. Mass Spectrom. 11 (1984) 601.
[55] K. Biemann, Methods Enzymol. 193 (1990) 886.
[56] A.H. Payne, J.H. Chelf, G.L. Glish, Analyst 125 (2000) 635.
[57] A.R. Dongré, J.L. Jones, A. Somogyi, V.H. Wysocki, J. Am. Chem. Soc. 118 (1996) 8365.
[58] G. Tsaprailis, H. Nair, A. Somogyi, V.H. Wysocki, W. Zhong, J.H. Futrell, S.G. Summerfield, S.J. Gaskell, J. Am. Chem. Soc. 121 (1999) 5142.
[59] G. Tsaprailis, A. Somogyi, E.N. Nikolaev, V.H. Wysocki, Int. J. Mass Spectrom. 195/196 (2000) 467.
[60] L. Rovatti, B. Masin, S. Catinella, M. Hamdan, Rapid Commun. Mass Spectrom. 11 (1997) 1223.
[61] R.W. Vachet, B.M. Bishop, B.W. Erickson, G.L. Glish, J. Am. Chem. Soc. 119 (1997) 5481.
[62] A. Klug, J.W.R. Schwabe, FASEB J. 9 (1995) 597.
[63] H. Lavanant, E. Hecquet, Y. Hopilliard, Int. J. Mass Spectrom. 185–187 (1999) 11.
[64] J. El Yazal, Y.-P. Pang, J. Phys. Chem. B 103 (1999) 8773.
[65] J. El Yazal, R.R. Roe, Y.-P. Pang, J. Phys. Chem. B 104 (2000) 6662.
[66] J. El Yazal, Y.-P. Pang, J. Phys. Chem. B 104 (2000) 6499.
[67] M. Peschke, A.T. Blades, P. Kebarle, J. Am. Chem. Soc. 122 (2000) 1492.
[68] F. Rogalewicz, Y. Hopilliard, G. Ohanessian, Int. J. Mass Spectrom. 206 (2001) 45.
[69] Y. Hopilliard, F. Rogalewicz, G. Ohanessian, Int. J. Mass Spectrom. 204 (2000) 267.
[70] F. Rogalewicz, Y. Hopilliard, G. Ohanessian, Int. J. Mass Spectrom. 201 (2000) 307.
[71] R.A.J. O'Hair, J.H. Bowie, S. Gronert, Int. J. Mass Spectrom. Ion Process. 117 (1992) 23.
[72] P.F. Hu, M.L. Gross, J. Am. Soc. Mass Spectrom. 5 (1994) 137.
[73] H. Zhao, A. Reiter, L.M. Teesch, J. Adams, J. Am. Chem. Soc. 115 (1993) 2854.